THE JOURNAL OF PHYSICAL CHEMISTRY C
A JOURNAL OF THE AMERICAN CHEMICAL SOCIETY

pubs.acs.org/JPCC

Article

Tuning Short Contacts between Polymer Chains To Enhance Charge Transport in Amorphous Donor−Acceptor Polymers

Published as part of The Journal of Physical Chemistry virtual special issue "Quantum Coherent Phenomena in Energy Harvesting and Storage".

Rishat Dilmurat, Vincent Lemaur, Yoann Olivier, Sai Manoj Gali,* and David Beljonne*

Cite This: *J. Phys. Chem. C* 2022, 126, 3118−3126

Read Online

ACCESS | Metrics & More | Article Recommendations | Supporting Information

ABSTRACT: The design of semiconducting polymers with optimal charge transport characteristics has been at the crux of scientific research during the recent decades. While increase in crystalline order and planar conjugated backbones were demonstrated to be the key to success, they are not always mandatory. Sometimes, the charge carrier mobility can be enhanced by selecting conjugated backbones that are resilient to thermal fluctuations, despite leading to poor structural order. Herein, by coupling all-atom molecular dynamics simulations, electronic structure calculations, and kinetic Monte Carlo charge transport simulations, we demonstrate that the charge carrier mobility in amorphous donor−acceptor conjugated polymers is controlled by the density and quality of close-contact points between the chains and that the latter varies with the size of the donor block and the resulting alkyl side-chain density. We show an application of this strategy to the high-mobility poly(indacenodithiophene-*alt*-benzothiadiazole) (IDTBT) and poly(dithiopheneindenofluorene-*alt*-benzothiadiazole) (TIFBT) copolymers.

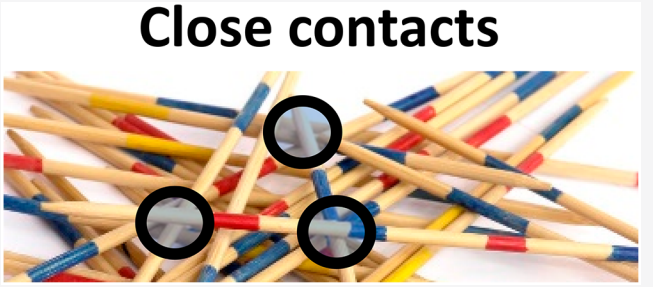

INTRODUCTION

Organic semiconductors, due to their ease of synthesis and low production costs combined with their crystalline order and high charge carrier mobility, are rapidly evolving as promising materials for applications in solar cells, light emitting diodes, and field effect transistors.[1−3] Molecular single crystals such as pentacene, TIPs-pentacene, rubrene, [1]benzothieno[3,2-*b*]-benzothiophene (BTBT), etc. are some of the most widely studied crystalline organic semiconductors as they show high charge carrier mobilities attributed to the presence of (transiently) delocalized electronic states.[4−8] But difficulty in processing of single crystals and the attainable size of the crystallites often limit their device utility. Comparatively, conjugated semiconducting polymers with their soft molecular nature and high conformational freedom of the building blocks ease solution processability allowing for large-scale/large-area applications. However, thin films made of conjugated polymers constitute ensembles of microdomains and/or aggregates with limited/short-range crystalline connected through amorphous domains. This extrinsic structural disorder results in localized transport states, which limits their charge transport characteristics.[9−11] Materials design strategies were aimed at increasing the (semi)crystallinity of these conjugated semiconducting polymers in order to increase the long-range crystalline order. Earlier investigations demonstrate that this is attainable by tailoring the functional (sub)units of the conjugated backbone of the polymers such as the (i) chemical structure of monomer unit, (ii) length and nature of alkyl side chains, and (iii) modulation of the conformational dynamics of the conjugated polymeric backbone.[12−18] However, recent studies indicate that the charge transport in organic semiconducting polymers is not necessarily dictated by the degree of crystallinity. The presence of aggregates with short-range order and/or interconnected domains within a globally amorphous polymeric domain will favor interchain charge transport.[9−11] Evidently, intrachain transport may prevail over short distances (along the polymer backbone) resulting in high charge carrier mobilities of the order of 10−100 $cm^2/(V\ s)$,[19] but it is often the interchain motion of the charge carriers, namely, their ability to hop between adjacent chains, that limits the mobility attainable at the mesoscopic device scales.[20−23] A recent comprehensive spectroscopic investigation of polymers with low degree of structural/crystalline order, such as poly-

Received: November 10, 2021
Revised: January 25, 2022
Published: February 2, 2022

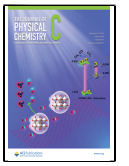

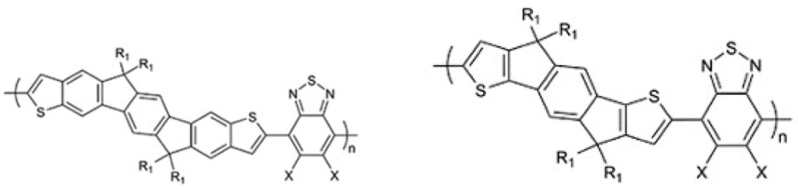

(a) TIFBT (b) IDTBT

Figure 1. Schematic chemical structures of the TIFBT (a) and IDTBT (b) polymers used in this work (R_1 = $C_{16}H_{33}$ and X = H).

(indacenodithiophene-*alt*-benzothiadiazole) (IDTBT) and poly(dithiopheneindenofluorene-*alt*-benzothiadiazole) (TIFBT), identified spectral fingerprints associated with close point contacts between running polymer chains. It was hypothesized that these crossing regions are involved in the long-range motion of the charge carriers.[24] It is also well established that restricting the conformational degrees of freedom by an appropriate selection of molecular subunits is beneficial to charge transport because of the resulting low-energy disorder.[25] In this regard, both IDTBT and TIFBT meet the requirement for resilience to conformational disorder and offer a nice playground to identify useful structure−property relationships between the nature of the functional group in the copolymer, the associated density of close contact points, and the resulting charge carrier mobility. To elucidate these aspects, we combine all-atom molecular mechanics and molecular dynamics simulations (MM/MD), ab initio electronic structure calculations, and kinetic Monte Carlo charge transport simulations to demonstrate that charge transport in IDTBT and TIFBT polymers is indeed sensitive to the density of contact points and the quality of interchain crossings.

COMPUTATIONAL DETAILS

Molecular Dynamics Simulations. To get insights on the impact of molecular subunits in modulating the charge transport characteristics, the supramolecular organization of the amorphous phases of TIFBT and IDTBT films (see Figure 1 for schematic chemical structures) has been first simulated following the protocol described in our previous work.[25] This strategy, briefly elucidated here, incorporates the coupling of molecular mechanics (MM) and molecular dynamics (MD) simulations on a large unit cell (300 Å × 300 Å × 300 Å) containing 24 randomly oriented ∼160 Å long oligomers (n = 8 for TIFTBT and n = 10 for IDTBT) that is replicated using periodic boundary conditions to build the 3D solid. We note that experimental investigations suggest physical polymer chain lengths that range from $n \approx 30$ to $n \approx 60$ monomer units in IDTBT and TIFBT polymers.[26−28] Besides, these studies have shown that the hole mobility increases with polymer weight. Because of computational constraints, the physical lengths used in the simulations are thus significantly smaller, which is likely the origin for underestimated theoretical mobility values compared to their experimental counterparts; see below. All MM/MD calculations have been performed with the Materials Studio (MS) 2018 package using a force-field derived from Dreiding[24,25,29] where the torsion potentials between adjacent subunits and between the conjugated cores and the alkyl chains have been reparameterized against density functional theory (DFT) calculations (at the B3LYP/cc-pVTZ level of theory) performed using the Gaussian 09 suite. The atomic charges have been obtained by fitting the electrostatic potential (ESP charges) on an isolated dimer, calculated at the same level of theory. Once the unit cell is built, it is subjected to a 500 ps MD run at high temperature (*NVT*; T = 1000 K) while keeping the density low (∼0.02 g/cm^3) to favor a random spatial distribution of the oligomers. Then, five successive 500 ps long MD runs (*NPT*, P = 1 atm) were performed at decreasing temperature (1000K, 500 K, 400 K, 350 K, 300 K), and finally, a 2 ns long MD simulation (*NPT*; P = 1 atm, T = 300 K) is performed. Indeed, as reported previously by some of us, the polymer morphologies extracted from the above MD simulation protocol are found to be in reasonable agreement with the X-ray simulated results for a disordered phase and the experimental 2D-GIWAXS data.[30] Snapshots of the MD morphologies are saved every 20 ps for further analysis. To characterize the distance between the chains or their subunits (TIF, IDT, and/or BT), the radial distribution functions between the different subunits have been built from the 100 snapshots of the 2 ns long MD trajectory, taking as reference points different regions of the donor and/or acceptor; see Supporting Information Figure S1 for details. Finally, a density of interchain contacts between the subunits for IDTBT and TIFBT has been estimated by calculating the distance between each atom of the donor and/or acceptor groups belonging to different polymer chains for all of the 100 snapshots of the analysis MD trajectory.

Charge Transport Simulations. We determine the charge carrier mobility using kinetic Monte Carlo (KMC) simulations performed on the basis atomistic morphologies of amorphous TIFBT and IDTBT films from MM/MD simulations. In these KMC simulations, we consider that the rate of the elementary charge transfer processes are obtained in the framework of the semiclassical Marcus−Levich−Jortner (MLJ) theory,

$$k_{ij} = \frac{2\pi}{\hbar}\frac{J_{ij}^{\ 2}}{\sqrt{4\pi\lambda_S k_B T}} \sum_{n=0}^{\infty} \exp(-S_{\text{eff}})\frac{S_{\text{eff}}^{n}}{n!} \exp\left\{-\frac{(\Delta G_{ij} + \lambda_i + n\hbar\omega_{\text{eff}})^2}{4\lambda_S k_B T}\right\} \quad (1)$$

with

$$\Delta G_{ij} = \epsilon_j - \epsilon_i \pm e\vec{E}\cdot\vec{R}_{ij} \quad (2)$$

where T is the temperature and k_B is the Boltzmann constant, with temperature (T) set to 300 K in all the KMC simulations such that k_BT is around 25 meV. J_{ij} is the electronic coupling (transfer integral) between the hopping sites "i" and "j", which are the different monomer units of the polymeric system at the crossing points that are dynamically involved in the charge transfer process. The total reorganization energy λ is a combination of the (i) internal contribution (λ_i) associated with the change in geometry of the molecules upon charge

https://doi.org/10.1021/acs.jpcc.1c09711
J. Phys. Chem. C 2022, 126, 3118−3126

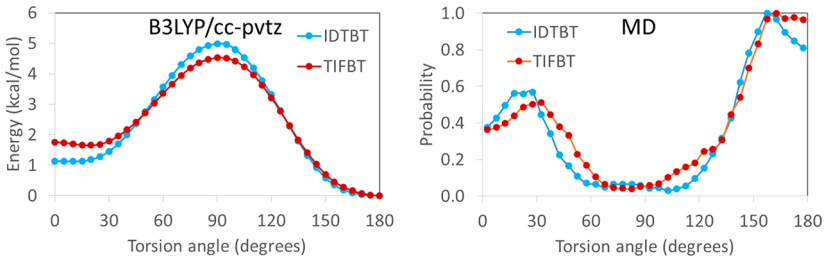

Figure 2. DFT(B3LYP/cc-pVTZ)-calculated gas-phase torsion potentials between the donor and acceptor fragments within an IDTBT (blue) and TIFBT (red) monomer (left). Torsion distribution profiles of IDTBT (blue) and TIFBT (red) were averaged over all the interring torsions along the polymer chains extracted from 2 ns long analysis MD (right).

transfer and (ii) external contribution (λ_s) the change in the polarization shell around the molecules involved in the charge transfer process. S_{eff} is the Huang−Rhys (HR) factor describing the strength of electron−vibration coupling associated with a single effective vibrational mode of energy $\hbar\omega_{eff}$. ΔG_{ij} (given by eq 2) represents the free energy change associated with the hole or electron transfer under the influence of electric field $\vec{E}$ from hopping site "i" to "j" with respective site energies of "ϵ_i" and "ϵ_j" and separated by a distance $\vec{R}_{ij}$, with "e" being the elementary charge. Interchain hole transfer integrals J_{ij} were calculated at the DFT/B3LYP/cc-pvdz level of theory by employing the projection method based on the Lodwin's orthogonalization scheme involving the HOMO orbitals[31] of the monomer units, which are extracted from the polymer chains extracted from MD morphologies. The internal reorganization energy (λ_i) was calculated at the same level of theory using the four-point adiabatic potential approach[32−34] with the values of 78 and 108 meV for TIFBT and IDTBT, respectively, whereas external contribution to reorganization energy (λ_e) was set to 0.2 eV following previous investigations.[35,36] Herein, to describe the charge transport in these two polymeric systems, we account for both intrachain and interchain contributions. All the transfer rates were thus first computed from a given subunit (namely, IDT or BT for IDTBT, or TIF or BT for TIFBT) or hopping site "i" to all the available neighbor sites "j" with nonzero J_{ij} transfer integrals. In our charge transport simulations, we considered periodic boundary conditions to follow the propagation of a single hole carrier within a given MD configuration. The KMC simulations proceed through the following steps (see Figure S2 for a schematic representation of the simulation process): (1) A polymeric subunit from any of the polymer chains, identified as hopping site "$i^{\ddagger}$", was randomly selected to be the initial hopping site from which charge transport is initiated. (2) Instantaneous hopping times from all the subunits of the selected polymer chain to all the subunits of the neighboring polymer chains with nonzero transfer integrals are computed within the first reaction method algorithm according to the following equation:

$$\tau_{ij} = \frac{1}{k_{ij}} \ln(r) \tag{3}$$

where τ_{ij} is defined as the time for a hole to hop from donor site "i" to acceptor site "j" using previously obtained transfer rates k_{ij} and "r" is a random number drawn from a uniform distribution within the interval 0 and 1. (3) The subunit within the initial polymer chain with the smallest of hopping time τ_{ij} is selected and is identified as the site from which interchain transfer occurs, whereas the coupled monomer unit on the neighboring polymer chain is identified as hopping site "j". (4) Before the interchain process takes place, the charge is first moved along the polymer chain (i.e., the intrachain charge transfer process) from initial monomer (hopping) unit "$i^{\ddagger}$" to the monomer unit "i" and the distance "$d_{i^{\ddagger}i}$" between these two sites is recorded. (5) The charge is moved from the hopping site "i" of the initial polymeric chain to the hopping site "j" of the neighboring polymeric chain, and the interchain hopping distance "d_{ij}" between the sites "i" and "j" (i.e., interchain charge transfer process) is added to the intrachain hopping distance "$d_{i^{\ddagger}i}$". The total distance is then updated. The total hopping time of the simulation is advanced by τ which is the sum of the intrachain $\tau_{i^{\ddagger}i}$ and interchain charge transfer time τ_{ij}, namely, $\tau = \tau_{ij} + \tau_{i^{\ddagger}i}$. On the basis of recent theoretical investigations,[14,19] a unique effective dwell time of 0.1 fs (1×10^{-14} s), which is the characteristic time associated with the charge (exciton) delocalization along a polymeric unit, was taken as the time $\tau_{i^{\ddagger}i}$ associated with intrachain charge transfer between sites "$i^{\ddagger}$" and "i" within the same polymeric chain irrespective of the intrachain distance covered by the hole. At the end of step 5, the hopping site "j" becomes the new hopping "$i^{\ddagger}$" from which the next KMC cycle starts. Steps 1−5 are then repeated so that until equilibrium was reached, namely, when the total simulation (diffusion) time (τ_k) reaches 100 μs, similar to previous works.[35,37]

For each MD sample considered, KMC simulations were performed with the electric field vector oriented along the "x", "y", and "z" box directions assuming a linear voltage drop across the sample and varying the electric field modulus from 0.1×10^5 V/cm to 2×10^5 V/cm. The mobility is obtained as

$$\mu_k = \frac{d}{|\vec{E}|} \frac{1}{\tau_k} \tag{4}$$

where τ_k is the total simulation time for a charge propagating in the direction of electric field $\vec{E}$ of norm $|\vec{E}|$ and "d" is the total distance traveled by the charge along the $\vec{E}$. "k" represents any given KMC simulation. The mobility values are taken as the average over 500 KMC simulations over "x", "y", "z" directions, performed on four different MD samples extracted at different MD simulation time steps.

RESULTS AND DISCUSSION

Structural Analysis. In the amorphous phase, the structural intrachain order, characterized by the interring torsion distribution profiles built from the 101 morphologies extracted along the MD trajectory, of IDTBT and TIFBT is rather similar (Figure 2). This was widely expected for weakly interacting molecules with similar gas-phase DFT-calculated torsion potentials and points out that extending the IDT unit

https://doi.org/10.1021/acs.jpcc.1c09711
J. Phys. Chem. C 2022, 126, 3118−3126

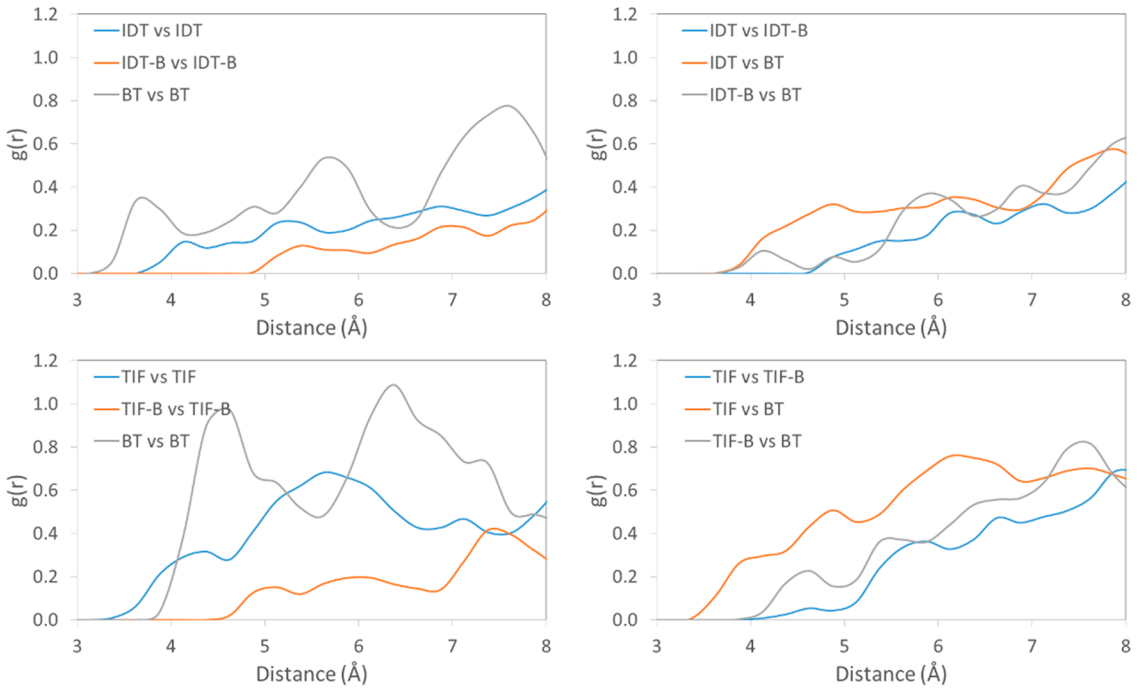

Figure 3. Radial distribution functions of neighboring contacts of IDTBT (upper panels) and TIFBT (lower panels) averaged over all molecular dynamics simulations. Neighboring contacts are defined in Supporting Information Figure S1.

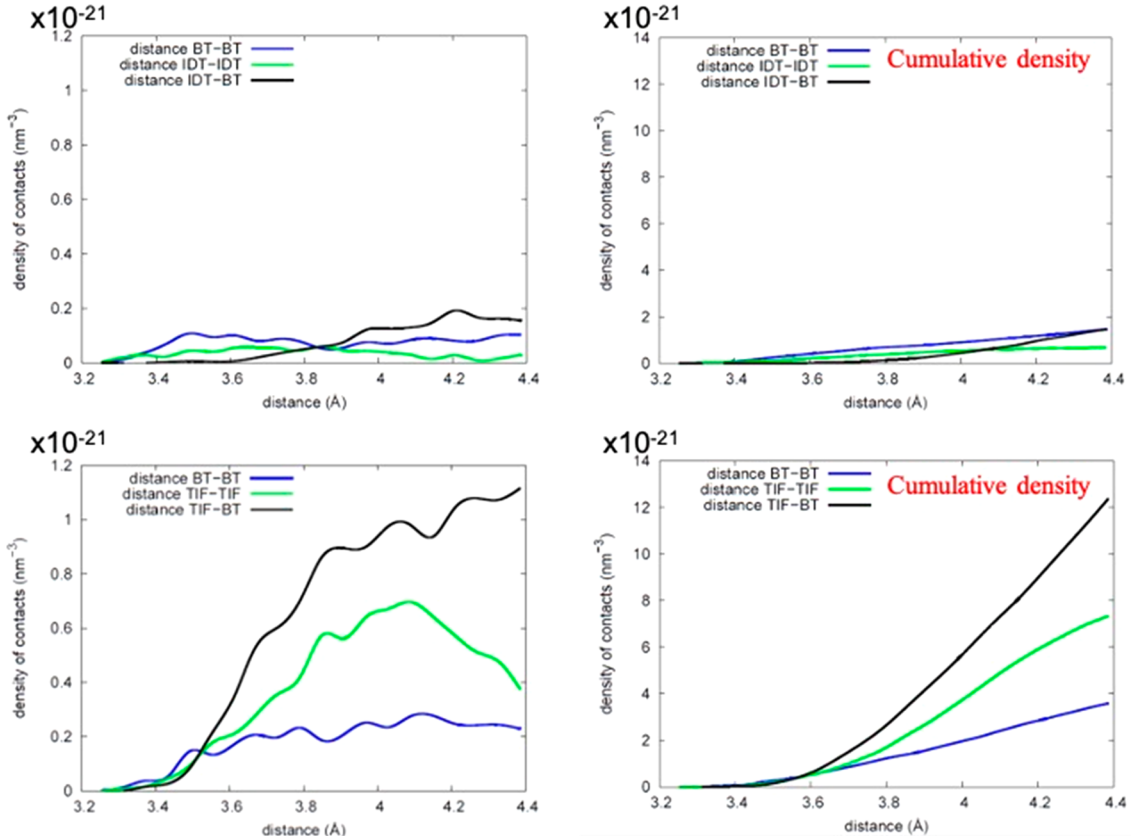

Figure 4. Density of contacts between neighboring subunits of IDTBT (upper panels) and TIFBT (lower panels) averaged over all the molecular dynamics simulations. The contacts are defined on the basis of four reference points located on each monomer subunits; see Supporting Information Figure S1.

into the TIF subunit by incorporating new conjugated fragments in the center of the molecule and keeping the peripheral rings intact is therefore not drastically affecting the intrachain structural order. Interestingly, inverted Boltzmann solid-state torsion potentials built from the MD trajectories (Figure S3) behave similarly to DFT gas phase torsion

https://doi.org/10.1021/acs.jpcc.1c09711
J. Phys. Chem. C 2022, 126, 3118−3126

potentials but with much smaller free enthalpy barriers. This translates into an increase of the small torsion angle populations (0−40°) with respect to that expected from gas phase torsion potentials.

Interchain charge transport is known to be strongly dependent on the quality and density of contact points between the polymer chains. To assess the density of contact points from a structural point of view, radial distribution functions between four characteristic reference points (see Figure S1 for details) were calculated along the MD trajectories. For IDTBT, due to the bulkiness of its alkyl side chains anchoring points, the central parts of the donor (IDT_B reference point) can only weakly interact with each other; their closest distance being always larger than ∼5 Å (Figure 3). Closer contacts are found when moving away from the center of the IDT unit. BT−BT contacts can be as close as ∼3.5 Å, while contacts involving the peripheral thiophene ring of the IDT unit can go down to ∼4 Å.

The supramolecular organization of TIFBT chains is different from that of IDTBT in the amorphous phase. Here, the closest contacts systematically involve the peripheral rings of the TIF unit. Indeed, due to the elongated shape of the TIF fragment, the peripheral rings are less influenced by the presence of the bulky center of the TIF subunit, and this allows closer interactions both with each other and with the BT fragment (distances down to 3.5 Å). This behavior could not have been anticipated on the basis of the torsion angle analysis since only small differences were found between the two polymers.

Regarding the density of contact points, our simulations reveal that the close crossing points are much more numerous in TIFBT compared to IDTBT; the total density of contacts smaller than 4 Å amounts to 10.4 contacts nm^{-3} and 1.78 contacts nm^{-3} for TIFBT and IDTBT, respectively; see Figure 4. Since most of the close contacts involve the peripheral rings of the TIF donor unit, this result suggests a stronger interconnection between the TIFBT chains that clearly finds its origin in the elongated shape of the donor unit.

Charge Transport Parameters. Previous theoretical investigations on charge transport in organic semiconducting systems emphasize that the charge carrier mobility is significantly influenced by (i) the fluctuations in site energies in the sample, which generate the diagonal component of energetic disorder,[38−43] and (ii) the fluctuations in the transfer integrals, which generate the off-diagonal component of energetic disorder[36,44−46] arising due to variation in the relative position of the molecules due to thermal fluctuations. Therefore, we analyzed the energetic disorder (diagonal and off-diagonal components) in the MD samples by considering a physical observable "A" calculated for "N" molecules along the MD trajectory[47] generating a static disorder (σ_A^{Stat}) given by

$$\sigma_A^{Stat} = \sqrt{\frac{\sum_n (\overline{A_n} - \overline{A})^2}{N}} \tag{5}$$

where the sum runs over the number of molecules, $\overline{A_n}$ is the average calculated along the molecular dynamics trajectory of the observable "A" calculated for the molecule n, $\overline{A}$ is the average over both the set of N molecules and I configurations of the MD trajectory. Similarly, the standard deviation of the dynamic disorder (σ_A^{Dyn}) for the observable is given by

$$\sigma_A^{Dyn} = \sqrt{\frac{\sum_i \sum_n (\overline{A_{n,i}} - \overline{A}_n)^2}{NI}} \tag{6}$$

where the sum runs over both the set of N molecules and the I snapshots and $A_{n,i}$ is the value of the observable for molecule "n" at snapshots "I". The observables "A" under consideration here are the site energies (ϵ) and transfer integrals (J), with σ_ϵ being the disorder on site energies and σ_J being the disorder on transfer integrals representing the off-diagonal disorder. Accordingly, σ_ϵ^{Stat} values for TIFBT and IDTBT are 67 and 90 meV, respectively, whereas σ_ϵ^{Dyn} values are 92 and 111 meV, respectively. A similar approach was used to compute the transfer integral fluctuations, with σ_J^{Stat} for TIFBT and IDTBT being of the order of ≈12 meV and ≈7 meV, respectively, whereas those of σ_J^{Dyn} are of the order of ≈4 meV and ≈3 meV, respectively. The static and dynamic components of energetic disorder are reported in Supporting Information Figures S4 and S5. In our KMC simulations, we included the contribution from both the diagonal and off-diagonal components of energetic disorder such that the static component of disorder ($\sigma_{\epsilon,J}^{Stat}$, extracted from eq 5) accounts for the energetic fluctuations within every given MD frame/snapshot (i.e., spatial fluctuations) and the dynamic component of disorder ($\sigma_{\epsilon,J}^{Dyn}$, extracted from eq 6) accounts for the energetic fluctuations over different MD frames separated in time (i.e., temporal fluctuations). Following our recent investigations[25,48] the total diagonal (σ_ϵ) and off-diagonal (σ_J) components of energetic disorder employed in this work were extracted using eq 7. While the diagonal component of energetic disorder in IDTBT samples is larger in magnitude than in TIFBT samples with respective σ_ϵ values of ≈143 meV and ≈114 meV, the off-diagonal component of disorder is approximately similar in both of the samples with TIFBT showing marginally higher average values of transfer integrals with respective σ_J values of ≈12 meV and ≈8 meV.

$$\sigma_\epsilon = \sqrt{(\sigma_\epsilon^{Stat})^2 + (\sigma_\epsilon^{Dyn})^2}$$
$$\sigma_J = \sqrt{(\sigma_{J_{ij}}^{Stat})^2 + (\sigma_{J_{ij}}^{Dyn})^2} \tag{7}$$

We further analyzed the electronic connectivity[48] which is defined as the number $n(J_{th})$ of neighbor molecules "j" coupled to a given molecule "i" with the electronic coupling "J" larger than the a given threshold value J_{th}. As both TIFBT and IDTBT show few neighbors with large transfer integral values, the electronic connectivity tends to reach zero for transfer integrals greater than 20 meV, as reported in Figure 5.

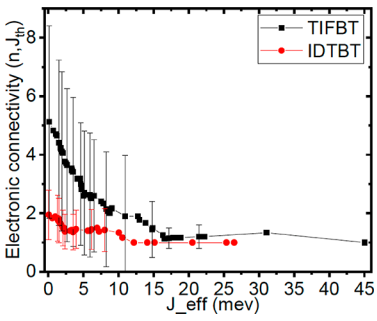

Figure 5. Electronic connectivity of TIFBT (in black) and IDTBT (in red) as a function of transfer integrals, with the corresponding errors bars.

https://doi.org/10.1021/acs.jpcc.1c09711
J. Phys. Chem. C 2022, 126, 3118−3126

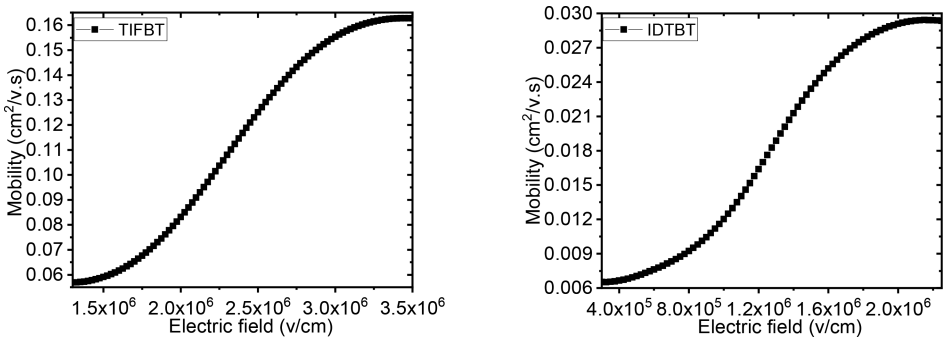

Figure 6. Electric-field dependent charge carrier mobility in TIFBT (left) and IDTBT (right), as obtained from KMC simulations.

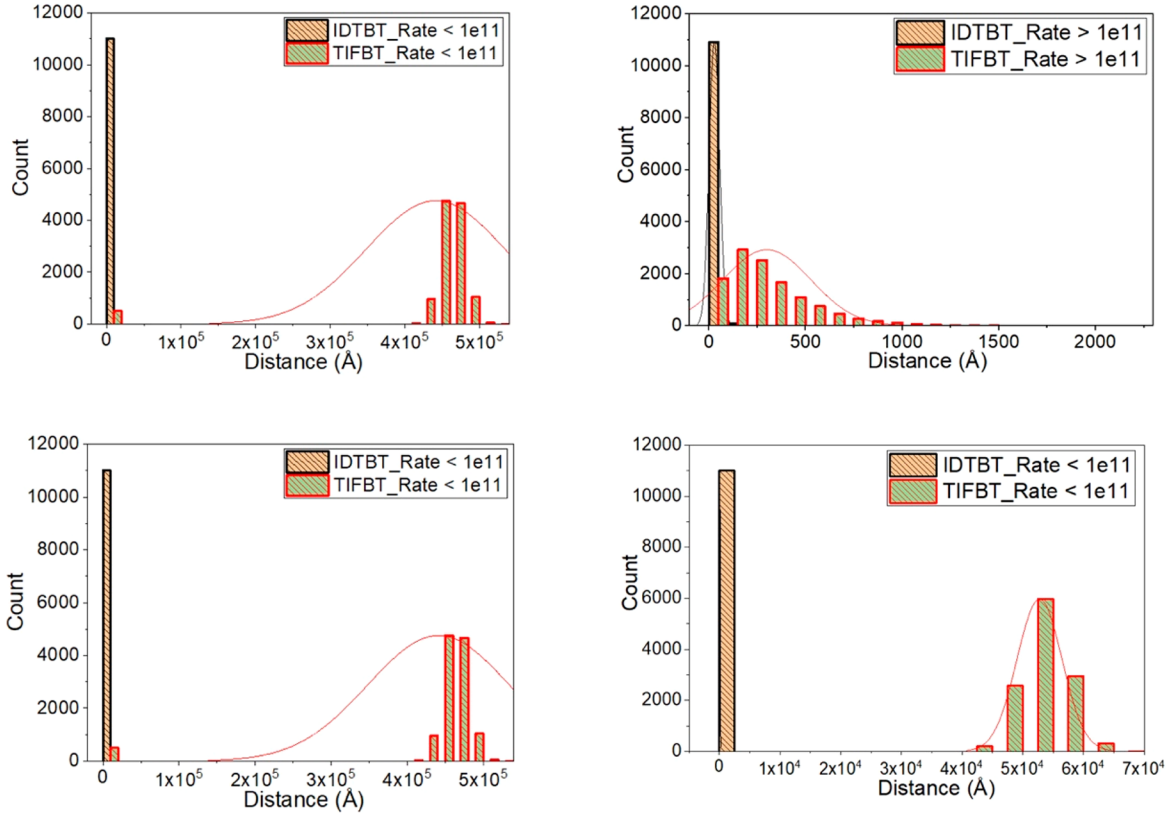

Figure 7. Percolation pathways associated with two different range of charge carrier hopping rates (left and right), as obtained for two randomly selected MD snapshots (top and bottom).

However, we observed that the electronic connectivity of TIFBT is substantially larger than IDTBT for threshold J values below 15 meV, indicating that the electronic coordination between neighboring molecules in the former is far greater, which could potentially lead to a larger number of charge percolation pathways. This is also consistent with the total number of calculated transfer integrals, which is much larger for TIFBT (≈42 000) compared to IDTBT (≈18 000). In addition, the larger electronic connectivity observed in TIFBT, in comparison to the IDTBT, clearly follows the larger number of closer contacts observed in TIFBT as in Figure 4, with the higher density of TIF-TIF and TIF-BT contacts along with the elongated unit length of TIF moiety contributing toward the enhanced intermolecular connectivity.

Charge Carrier Mobility. Having analyzed the microscopic parameters that could influence the charge carrier mobilities of TIFBT and IDTBT, we performed KMC simulations following the procedure described above and by including both the energetic and positional components of disorders. More specifically, the diagonal disorder was introduced by initializing the ϵ_i and ϵ_j values in eq 2 at the beginning of every KMC run by random sampling from a Gaussian distribution with standard deviation of σ_ϵ centered on zero, whereas the contribution of off-diagonal (positional) disorder was incorporated at the beginning of every KMC run by replacing the mean transfer integral value of J_{ij}^2 in eq 1 by the mean squared transfer integral value $\langle J_{ij}^2 \rangle$ $(=\langle J_{ij} \rangle^2 + \sigma_J^2)$ which corresponds to a thermalized value of the transfer integral. These simulation conditions were considered as they are known to often provide theoretical mobility estimates that are in semiquantitative agreement with experimental observations.[25,46,48,49]

In Figure 6, we report the electric field dependence of the hole mobility for both polymers. The hole mobility of TIFBT

https://doi.org/10.1021/acs.jpcc.1c09711
J. Phys. Chem. C 2022, 126, 3118−3126

at the high electric fields are of the order of ≈0.16 $cm^2/(V\ s)$, whereas that of IDTBT are of the order of ≈0.03 $cm^2/(V\ s)$. When extrapolated to zero electric field considering a Poole−Frenkel trap-assisted charge transport mechanism with

$$\mu(E) = \mu_0 \exp(\beta\sqrt{E})$$

where β is the Poole−Frenkle factor, the zero-field mobility (μ_0) values for TIFBT remain 1 order of magnitude larger than that of IDTBT, with the approximate values of 0.025 $cm^2/(V\ s)$ and 0.001 $cm^2/(V\ s)$, respectively. The lower hole mobility for IDTBT compared to TIFBT can be partly related to the comparatively lower transfer integral values and higher diagonal disorder in IDTBT samples. However, the poorer electronic connectivity in IDTBT likely dominates the difference in (zero-field) mobility between the two polymers. As a result, in TIFBT more percolation pathways are enabled for efficient charge transport, analogous to the random resistance network for charge transport in organic semiconductors.[3] To validate the presence of percolation pathways and its subsequent impact in modulating the charge carrier mobilities in TIFBT samples in comparison to that of IDTBT, the average distance covered by a charge carrier hopping between molecular sites within a given range of hopping rates is computed. We run two types of KMC simulations considering only the hopping rates k_{ij} larger than 1×10^{11} s^{-1} or the $k_{ij} < 1 \times 10^{11}$ s^{-1} for both TIFBT and IDTBT systems, similarly as in ref 43. The cutoff transfer rate value of 1×10^{11} s^{-1} was taken as a proxy based on the average of KMC hopping rates observed in both TIFBT and IDTBT samples, as reported in Figure S6.

The distance traveled by the charge carriers in TIFBT and IDTBT samples for a given hopping rate, for two different MD snapshots that are separated in time and randomly selected, is reported in Figure 7. Irrespective of the cutoff hopping rate selected, the average distance traveled by the charge carriers (holes) in TIFBT samples is evidently larger and show a broader distribution compared to IDTBT, implying the existence of more long-distance continuous pathways in TIFBT samples. The charge carriers can efficiently funnel resulting in higher mobilities in TIFBT than in IDTBT, as reported in Figure 6. It is to be noted, however, that although the hole mobilities of both TIFBT and IDTBT systems (of the order of ≈0.16 $cm^2/(V\ s)$ and 0.03 $cm^2/(V\ s)$, respectively) show a trend in agreement with recent experimental observations,[24,25] the theoretical absolute values are smaller than the experimental data. The experimental field effect mobilities of TIFBT and IDTBT according to recent experimental investigations are of the order of ≈3 $cm^2/(V\ s)$ and ≈1 $cm^2/(V\ s)$, respectively.[24,25] Three major aspects could be considered as the contributing factors toward these differences: (i) The parameters for energetic disorder considered in the KMC simulations could play a key role in governing the absolute magnitude of mobilities extracted in this work. Indeed, modulating these parameters within the acceptable values can modify the magnitude of charge carrier mobilities as shown in Figures S7 and S8. However, as elaborated in Figures S7 and S8, even after implementing different disorder models by varying the simulation conditions, the hole mobilities in TIFBT samples are approximately 1 order of magnitude larger when compared to IDTBT samples. (ii) The presence of semicrystalline domains in experimental samples as against the completely amorphous morphologies considered in this work for both TIFBT and IDTBT samples could also explain part of the discrepancy and (iii) the difference in absolute values in the length of polymer chain used in the simulations as against polymer chain lengths present in experimental samples. Incorporating longer polymer chains in simulations could increase the number of available fast transport pathways along the polymer chains and would increase the isotropic mobility values by promoting intrachain transport. Nevertheless, the semiquantitative agreement with experiments, with TIFBT showing higher hole mobility values when compared to IDTBT, coupled with its connectivity-enabled percolation pathways to efficiently funnel the charge carriers, clearly shows that it is indeed the density of contact points between molecular sites involved in the charge transport that plays a significant role in modulating the charge transport properties, irrespective of the degree of interchain structural order.

CONCLUSIONS

We present a theoretical study of charge transport in poly(indacenodithiophene-*alt*-benzothiadiazole) (IDTBT) and poly(dithiopheneindenofluorene-*alt*-benzothiadiazole) (TIFBT) polymers, which show similar conformational resilience to torsions but differ in the functional subunits. The electric field dependent hole mobilities were extracted from kinetic Monte Carlo (KMC) simulations performed on TIFBT and IDTBT polymer morphologies built from full atomistic molecular dynamic simulations, with charge hopping parameters extracted from subsequent quantum chemistry calculations on the molecules and/or dimers obtained from these MD morphologies. TIFBT shows substantially larger mobilities with respect to IDTBT, owing not only to the comparatively higher transfer integral values but also to the higher degree of electronic connectivity. Both effects are favored by the nature of the TIF units, wherein the elongated shape and the bulkiness of the TIF fragment promote a better interaction between the peripheral thiophene rings and thus a higher density of close contacts. A higher electronic connectivity between neighboring units in turn favors the formation of percolation channels to efficiently transport the charge carriers, yielding increased charge carrier mobilities for TIFBT with respect to IDTBT. This work, therefore, demonstrates that a selective functionalization of the molecular subunits can not only preserve the conformational resilience to thermal fluctuations but also play a significant role in modulating the density of contact points between neighboring molecules, thereby enhancing the charge carrier mobilities, irrespective of the degree of semicrystalline order prevalent in organic semiconducting polymers.

ASSOCIATED CONTENT

Supporting Information

The Supporting Information is available free of charge at https://pubs.acs.org/doi/10.1021/acs.jpcc.1c09711.

Schematic representation of molecular subunits of IDTBT and TIFBT systems, schematic representation of charge transport model employed in this work, distribution of torsion potentials, electronic site energies and transfer integrals, and the charge carrier mobilities obtained under different simulations conditions (PDF)

https://doi.org/10.1021/acs.jpcc.1c09711
J. Phys. Chem. C 2022, 126, 3118−3126

AUTHOR INFORMATION

Corresponding Authors

Sai Manoj Gali − *Laboratory for Chemistry of Novel Materials, Materials Research Institute, University of Mons, 7000 Mons, Belgium;* orcid.org/0000-0002-0388-7888; Email: saimanoj.gai@umons.ac.be

David Beljonne − *Laboratory for Chemistry of Novel Materials, Materials Research Institute, University of Mons, 7000 Mons, Belgium;* orcid.org/0000-0002-2989-3557; Email: david.beljonne@umons.ac.be

Authors

Rishat Dilmurat − *Laboratory for Chemistry of Novel Materials, Materials Research Institute, University of Mons, 7000 Mons, Belgium*

Vincent Lemaur − *Laboratory for Chemistry of Novel Materials, Materials Research Institute, University of Mons, 7000 Mons, Belgium*

Yoann Olivier − *Laboratory for Computational Modeling of Functional Materials, Namur Institute of Structured Matter, Université de Namur, 5000 Namur, Belgium*

Complete contact information is available at: https://pubs.acs.org/10.1021/acs.jpcc.1c09711

Notes

The authors declare no competing financial interest.

ACKNOWLEDGMENTS

This work was supported by the Belgian National Fund for Scientific Research (FRS-FNRS), the Consortium des Équipements de Calcul Intensif—CÉCI, under Grant 2.5020.11, and the Walloon Region (ZENOBE Tier-1 Supercomputer, under Grant 1117545). This work has received funding from the European Union's Horizon 2020 Research and Innovation Programme under Grant Agreement 964677. D.B. is FNRS Research Director.

REFERENCES

(1) Mas-Torrent, M.; Rovira, C. Role of Molecular Order and Solid-State Structure in Organic Field-Effect Transistors. *Chem. Rev.* **2011**, *111* (8), 4833−4856.

(2) Wang, C.; Dong, H.; Hu, W.; Liu, Y.; Zhu, D. Semiconducting π-Conjugated Systems in Field-Effect Transistors: A Material Odyssey of Organic Electronics. *Chem. Rev.* **2012**, *112* (4), 2208−2267.

(3) Sirringhaus, H. 25th Anniversary Article: Organic Field-Effect Transistors: The Path Beyond Amorphous Silicon. *Adv. Mater.* **2014**, *26* (9), 1319−1335.

(4) Takeyama, Y.; Ono, S.; Matsumoto, Y. Organic Single Crystal Transistor Characteristics of Single-Crystal Phase Pentacene Grown by Ionic Liquid-Assisted Vacuum Deposition. *Appl. Phys. Lett.* **2012**, *101* (8), No. 083303.

(5) Ling, M.-M.; Reese, C.; Briseno, A. L.; Bao, Z. Non-Destructive Probing of the Anisotropy of Field-Effect Mobility in the Rubrene Single Crystal. *Synth. Met.* **2007**, *157* (6−7), 257−260.

(6) Yuan, Y.; Giri, G.; Ayzner, A. L.; Zoombelt, A. P.; Mannsfeld, S. C. B.; Chen, J.; Nordlund, D.; Toney, M. F.; Huang, J.; Bao, Z. Ultra-High Mobility Transparent Organic Thin Film Transistors Grown by an off-Centre Spin-Coating Method. *Nat. Commun.* **2014**, *5* (1), 3005.

(7) Kobayashi, H.; Kobayashi, N.; Hosoi, S.; Koshitani, N.; Murakami, D.; Shirasawa, R.; Kudo, Y.; Hobara, D.; Tokita, Y.; Itabashi, M. Hopping and Band Mobilities of Pentacene, Rubrene, and 2,7-Dioctyl[1]Benzothieno[3,2- b][1]Benzothiophene (C 8 -BTBT) from First Principle Calculations. *J. Chem. Phys.* **2013**, *139* (1), No. 014707.

(8) Schweicher, G.; Lemaur, V.; Niebel, C.; Ruzié, C.; Diao, Y.; Goto, O.; Lee, W.-Y.; Kim, Y.; Arlin, J.-B.; Karpinska, J.; et al. Bulky End-Capped [1]Benzothieno[3,2- b]Benzothiophenes: Reaching High-Mobility Organic Semiconductors by Fine Tuning of the Crystalline Solid-State Order. *Adv. Mater.* **2015**, *27* (19), 3066−3072.

(9) Noriega, R.; Rivnay, J.; Vandewal, K.; Koch, F. P. V.; Stingelin, N.; Smith, P.; Toney, M. F.; Salleo, A. A General Relationship between Disorder, Aggregation and Charge Transport in Conjugated Polymers. *Nat. Mater.* **2013**, *12* (11), 1038−1044.

(10) Wang, S.; Fabiano, S.; Himmelberger, S.; Puzinas, S.; Crispin, X.; Salleo, A.; Berggren, M. Experimental Evidence That Short-Range Intermolecular Aggregation Is Sufficient for Efficient Charge Transport in Conjugated Polymers. *Proc. Natl. Acad. Sci. U. S. A.* **2015**, *112* (34), 10599−10604.

(11) Son, S. Y.; Kim, Y.; Lee, J.; Lee, G.-Y.; Park, W.-T.; Noh, Y.-Y.; Park, C. E.; Park, T. High-Field-Effect Mobility of Low-Crystallinity Conjugated Polymers with Localized Aggregates. *J. Am. Chem. Soc.* **2016**, *138* (26), 8096−8103.

(12) Tsao, H. N.; Cho, D. M.; Park, I.; Hansen, M. R.; Mavrinskiy, A.; Yoon, D. Y.; Graf, R.; Pisula, W.; Spiess, H. W.; Müllen, K. Ultrahigh Mobility in Polymer Field-Effect Transistors by Design. *J. Am. Chem. Soc.* **2011**, *133* (8), 2605−2612.

(13) Wang, S.; Kappl, M.; Liebewirth, I.; Müller, M.; Kirchhoff, K.; Pisula, W.; Müllen, K. Organic Field-Effect Transistors Based on Highly Ordered Single Polymer Fibers. *Adv. Mater.* **2012**, *24* (3), 417−420.

(14) Noriega, R.; Salleo, A.; Spakowitz, A. J. Chain Conformations Dictate Multiscale Charge Transport Phenomena in Disordered Semiconducting Polymers. *Proc. Natl. Acad. Sci. U. S. A.* **2013**, *110* (41), 16315−16320.

(15) Kim, B. J.; Lee, H.-S.; Lee, J. S.; Cho, S.; Kim, H.; Son, H. J.; Kim, H.; Ko, M. J.; Park, S.; Kang, M. S.; et al. Correlation between Crystallinity, Charge Transport, and Electrical Stability in an Ambipolar Polymer Field-Effect Transistor Based on Poly-(Naphthalene- Alt -Diketopyrrolopyrrole). *J. Phys. Chem. C* **2013**, *117* (22), 11479−11486.

(16) Steyrleuthner, R.; Di Pietro, R.; Collins, B. A.; Polzer, F.; Himmelberger, S.; Schubert, M.; Chen, Z.; Zhang, S.; Salleo, A.; Ade, H.; et al. The Role of Regioregularity, Crystallinity, and Chain Orientation on Electron Transport in a High-Mobility n-Type Copolymer. *J. Am. Chem. Soc.* **2014**, *136* (11), 4245−4256.

(17) Oosterbaan, W. D.; Bolsée, J.-C.; Wang, L.; Vrindts, V.; Lutsen, L. J.; Lemaur, V.; Beljonne, D.; McNeill, C. R.; Thomsen, L.; Manca, J. V.; et al. On the Relation between Morphology and FET Mobility of Poly(3-Alkylthiophene)s at the Polymer/SiO 2 and Polymer/Air Interface. *Adv. Funct. Mater.* **2014**, *24* (14), 1994−2004.

(18) Mendels, D.; Tessler, N. A Comprehensive Study of the Effects of Chain Morphology on the Transport Properties of Amorphous Polymer Films. *Sci. Rep.* **2016**, *6* (1), 29092.

(19) Prodhan, S.; Qiu, J.; Ricci, M.; Roscioni, O. M.; Wang, L.; Beljonne, D. Design Rules to Maximize Charge-Carrier Mobility along Conjugated Polymer Chains. *J. Phys. Chem. Lett.* **2020**, *11* (16), 6519−6525.

(20) Athanasopoulos, S.; Kirkpatrick, J.; Martínez, D.; Frost, J. M.; Foden, C. M.; Walker, A. B.; Nelson, J. Predictive Study of Charge Transport in Disordered Semiconducting Polymers. *Nano Lett.* **2007**, *7*, 1785−1788.

(21) Carbone, P.; Troisi, A. Charge Diffusion in Semiconducting Polymers: Analytical Relation between Polymer Rigidity and Time Scales for Intrachain and Interchain Hopping. *J. Phys. Chem. Lett.* **2014**, *5*, 2637−2641.

(22) Noriega, R.; Rivnay, J.; Vandewal, K.; Koch, F. P. V.; Stingelin, N.; Smith, P.; Toney, M. F.; Salleo, A. A General Relationship between Disorder, Aggregation and Charge Transport in Conjugated Polymers. *Nat. Mater.* **2013**, *12* (11), 1038−1044.

(23) Troisi, A. The Speed Limit for Sequential Charge Hopping in Molecular Materials. *Org. Electron.* **2011**, *12* (12), 1988−1991.

(24) Thomas, T. H.; Harkin, D. J.; Gillett, A. J.; Lemaur, V.; Nikolka, M.; Sadhanala, A.; Richter, J. M.; Armitage, J.; Chen, H.; McCulloch,

I.; et al. Short Contacts between Chains Enhancing Luminescence Quantum Yields and Carrier Mobilities in Conjugated Copolymers. *Nat. Commun.* **2019**, *10* (1), 2614.
(25) Lemaur, V.; Cornil, J.; Lazzaroni, R.; Sirringhaus, H.; Beljonne, D.; Olivier, Y. Resilience to Conformational Fluctuations Controls Energetic Disorder in Conjugated Polymer Materials: Insights from Atomistic Simulations. *Chem. Mater.* **2019**, *31* (17), 6889−6899.
(26) Chen, H.; Hurhangee, M.; Nikolka, M.; Zhang, W.; Kirkus, M.; Neophytou, M.; Cryer, S. J.; Harkin, D.; Hayoz, P.; Abdi-Jalebi, M.; et al. Dithiopheneindenofluorene (TIF) Semiconducting Polymers with Very High Mobility in Field-Effect Transistors. *Adv. Mater.* **2017**, *29* (36), 1702523.
(27) Zhang, W.; Smith, J.; Watkins, S. E.; Gysel, R.; McGehee, M.; Salleo, A.; Kirkpatrick, J.; Ashraf, S.; Anthopoulos, T.; Heeney, M.; et al. Indacenodithiophene Semiconducting Polymers for High-Performance, Air-Stable Transistors. *J. Am. Chem. Soc.* **2010**, *132* (33), 11437−11439.
(28) Zhang, X.; Bronstein, H.; Kronemeijer, A. J.; Smith, J.; Kim, Y.; Kline, R. J.; Richter, L. J.; Anthopoulos, T. D.; Sirringhaus, H.; Song, K.; et al. Molecular Origin of High Field-Effect Mobility in an Indacenodithiophene−Benzothiadiazole Copolymer. *Nat. Commun.* **2013**, *4* (1), 2238.
(29) Mayo, S. L.; Olafson, B. D.; Goddard, W. A. DREIDING: A Generic Force Field for Molecular Simulations. *J. Phys. Chem.* **1990**, *94* (26), 8897−8909.
(30) Venkateshvaran, D.; Nikolka, M.; Sadhanala, A.; Lemaur, V.; Zelazny, M.; Kepa, M.; Hurhangee, M.; Kronemeijer, A. J.; Pecunia, V.; Nasrallah, I.; et al. Approaching Disorder-Free Transport in High-Mobility Conjugated Polymers. *Nature* **2014**, *515* (7527), 384−388.
(31) Viani, L.; Olivier, Y.; Athanasopoulos, S.; da Silva Filho, D. A.; Hulliger, J.; Brédas, J.-L.; Gierschner, J.; Cornil, J. Theoretical Characterization of Charge Transport in One-Dimensional Collinear Arrays of Organic Conjugated Molecules. *ChemPhysChem* **2010**, *11* (5), 1062−1068.
(32) Horowitz, G.; Kouki, F.; Spearman, P.; Fichou, D.; Nogues, C.; Pan, X.; Garnier, F. Evidence for N-Type Conduction in a Perylene Tetracarboxylic Diimide Derivative. *Adv. Mater.* **1996**, *8* (3), 242−245.
(33) Qian, H.; Negri, F.; Wang, C.; Wang, Z. Fully Conjugated Tri(Perylene Bisimides): An Approach to the Construction of n -Type Graphene Nanoribbons. *J. Am. Chem. Soc.* **2008**, *130* (52), 17970−17976.
(34) Schmidt-Mende, L.; Fechtenkotter, A.; Mullen, K.; Moons, E.; Friend, R. H.; MacKenzie, J. D. Self-Organized Discotic Liquid Crystals for High-Efficiency Organic Photovoltaics. *Science* **2001**, *293* (5532), 1119−1122.
(35) Olivier, Y.; Lemaur, V.; Brédas, J. L.; Cornil, J. Charge Hopping in Organic Semiconductors: Influence of Molecular Parameters on Macroscopic Mobilities in Model One-Dimensional Stacks. *J. Phys. Chem. A* **2006**, *110* (19), 6356−6364.
(36) Troisi, A.; Orlandi, G. Dynamics of the Intermolecular Transfer Integral in Crystalline Organic Semiconductors. *J. Phys. Chem. A* **2006**, *110* (11), 4065−4070.
(37) Coropceanu, V.; Cornil, J.; da Silva Filho, D. A.; Olivier, Y.; Silbey, R.; Brédas, J.-L. Charge Transport in Organic Semiconductors. *Chem. Rev.* **2007**, *107* (4), 926−952.
(38) Bässler, H. Charge Transport in Disordered Organic Photoconductors a {Monte Carlo} Simulation Study. *Phys. Status Solidi* **1993**, *175*, 15−56.
(39) Martinelli, N. G.; Savini, M.; Muccioli, L.; Olivier, Y.; Castet, F.; Zannoni, C.; Beljonne, D.; Cornil, J. Modeling Polymer Dielectric/Pentacene Interfaces: On the Role of Electrostatic Energy Disorder on Charge Carrier Mobility. *Adv. Funct. Mater.* **2009**, *19* (20), 3254−3261.
(40) Lukyanov, A.; Andrienko, D. Extracting Nondispersive Charge Carrier Mobilities of Organic Semiconductors from Simulations of Small Systems. *Phys. Rev. B* **2010**, *82* (19), 193202.
(41) Cornil, J.; Verlaak, S.; Martinelli, N.; Mityashin, A.; Olivier, Y.; Van Regemorter, T.; D'Avino, G.; Muccioli, L.; Zannoni, C.; Castet, F.; et al. Exploring the Energy Landscape of the Charge Transport Levels in Organic Semiconductors at the Molecular Scale. *Acc. Chem. Res.* **2013**, *46* (2), 434−443.
(42) Mityashin, A.; Roscioni, O. M.; Muccioli, L.; Zannoni, C.; Geskin, V.; Cornil, J.; Janssen, D.; Steudel, S.; Genoe, J.; Heremans, P. Multiscale Modeling of the Electrostatic Impact of Self-Assembled Monolayers Used as Gate Dielectric Treatment in Organic Thin-Film Transistors. *ACS Appl. Mater. Interfaces* **2014**, *6* (17), 15372−15378.
(43) D'Avino, G.; Olivier, Y.; Muccioli, L.; Beljonne, D. Do Charges Delocalize over Multiple Molecules in Fullerene Derivatives? *J. Mater. Chem. C* **2016**, *4* (17), 3747−3756.
(44) Martinelli, N. G.; Olivier, Y.; Athanasopoulos, S.; Ruiz Delgado, M.-C.; Pigg, K. R.; da Silva Filho, D. A.; Sánchez-Carrera, R. S.; Venuti, E.; Della Valle, R. G.; Brédas, J.-L.; et al. Influence of Intermolecular Vibrations on the Electronic Coupling in Organic Semiconductors: The Case of Anthracene and Perfluoropentacene. *ChemPhysChem* **2009**, *10* (13), 2265−2273.
(45) Sánchez-Carrera, R. S.; Paramonov, P.; Day, G. M.; Coropceanu, V.; Brédas, J.-L. Interaction of Charge Carriers with Lattice Vibrations in Oligoacene Crystals from Naphthalene to Pentacene. *J. Am. Chem. Soc.* **2010**, *132* (41), 14437−14446.
(46) Gali, S. M.; D'Avino, G.; Aurel, P.; Han, G.; Yi, Y.; Papadopoulos, T. A.; Coropceanu, V.; Brédas, J.-L.; Hadziioannou, G.; Zannoni, C.; et al. Energetic Fluctuations in Amorphous Semiconducting Polymers: Impact on Charge-Carrier Mobility. *J. Chem. Phys.* **2017**, *147* (13), 134904.
(47) Olivier, Y.; Yurash, B.; Muccioli, L.; D'Avino, G.; Mikhnenko, O.; Sancho-García, J. C.; Adachi, C.; Nguyen, T.-Q.; Beljonne, D. Nature of the Singlet and Triplet Excitations Mediating Thermally Activated Delayed Fluorescence. *Phys. Rev. Mater.* **2017**, *1* (7), No. 075602.
(48) Londi, G.; Dilmurat, R.; D'Avino, G.; Lemaur, V.; Olivier, Y.; Beljonne, D. Comprehensive Modelling Study of Singlet Exciton Diffusion in Donor−Acceptor Dyads: When Small Changes in Chemical Structure Matter. *Phys. Chem. Chem. Phys.* **2019**, *21* (45), 25023−25034.
(49) Gali, S. M.; Matta, M.; Lessard, B. H.; Castet, F.; Muccioli, L. Ambipolarity and Dimensionality of Charge Transport in Crystalline Group 14 Phthalocyanines: A Computational Study. *J. Phys. Chem. C* **2018**, *122* (5), 2554−2563.

https://doi.org/10.1021/acs.jpcc.1c09711
J. Phys. Chem. C 2022, 126, 3118−3126